


RESEARCH ARTICLE

Optimization of the nutritional environment for differentiation of human-induced pluripotent stem cells using design of experiments—A proof of concept

Patricia P. Esteban¹ | Hamza Patel² | Farlan Veraitch² | Rana Khalife² 

¹College of Health and Life Sciences, School of Biosciences, Aston University, Birmingham, UK

²Department of Biochemical Engineering, University College London, London, UK

Correspondence

Rana Khalife, Department of Biochemical Engineering, University College London, Torrington Place, London WC1E 7JE, UK.
Email: rana.khalife.13@ucl.ac.uk

Funding information

UCL's Department of Biochemical Engineering and IDB

Abstract

The utilization of human-induced pluripotent stem cells (hiPSCs) in cell therapy has a tremendous potential but faces many practical challenges, including costs associated with cell culture media and growth factors. There is an immediate need to establish an optimized culture platform to direct the differentiation of hiPSCs into germ layers in a defined nutritional microenvironment to generate cost-effective and robust therapeutics. The aim of this study was to identify the optimal nutritional environment by mimicking the in vivo concentrations of three key factors (glucose, pyruvate, and oxygen) during the spontaneous differentiation of hiPSCs derived from cord blood, which greatly differ from the in vitro expansion and differentiation scenarios. Moreover, we hypothesized that the high glucose, pyruvate, and oxygen concentrations found in typical growth media could inhibit the differentiation of certain lineages. A design of experiments was used to investigate the interaction between these three variables during the spontaneous differentiation of hiPSCs. We found that lower oxygen and glucose concentrations enhance the expression of mesodermal (Brachyury, KIF1A) and ectodermal (Nestin, β -Tubulin) markers. Our findings present a novel approach for efficient directed differentiation of hiPSCs through the manipulation of media components while simultaneously avoiding the usage of growth factors thus reducing costs.

KEYWORDS

design of experiments, germ layer differentiation, human-induced pluripotent stem cells

1 | INTRODUCTION

The field of stem cell research has expanded greatly since the discovery of induced pluripotent stem cells (iPSCs). Reprogramming adult somatic cells into iPSCs helped overcoming the ethical and immunological barriers associated with the use of embryonic stem cells (ESCs).^{1–3}

Yamanaka et al first reprogrammed mouse iPSCs from adult mouse fibroblasts via the introduction into the cell of four key transcription

factors (Yamanaka's factors): octamer-binding transcription factor 4 (OCT-4), sex determining region Y box 2 (SOX2), myelocytomatosis viral oncogene homologue (c-MYC), and Kruppel-like factor 4 (KLF4).³ Following this, human-iPSC (hiPSCs) was also generated by the addition of integrating retroviral vectors expressing the same genes.⁴ The discovery of hiPSCs led to the mitigation of ethical concerns related to hESCs¹ and the advancement of autologous cell therapy. The use of iPSCs in regenerative medicine is diverse and ranges from the treatment of Parkinson's disease,^{5,6} spinal cord injury,^{7,8} platelet deficiency⁹ to retinal and macular degeneration.¹⁰ Moreover, patient-specific iPSCs

Patricia P. Esteban and Rana Khalife are joint first authors.

This is an open access article under the terms of the Creative Commons Attribution-NonCommercial-NoDerivs License, which permits use and distribution in any medium, provided the original work is properly cited, the use is non-commercial and no modifications or adaptations are made.

© 2021 The Authors. *Biotechnology Progress* published by Wiley Periodicals LLC on behalf of American Institute of Chemical Engineers.

are used as a model to understand several diseases like amyotrophic lateral sclerosis,¹¹ Parkinson's disease,¹² Alzheimer's disease,^{13,14} and schizophrenia.¹⁵ Other iPSCs models have been generated for the treatment of adenosine deaminase deficiency-related severe combined immunodeficiency, Shwachman–Bodian–Diamond syndrome, Gaucher disease Type II, Duchenne and Becker muscular dystrophy, Parkinson disease, Huntington disease, juvenile-onset Type 1 diabetes mellitus, Down syndrome, and Lesch–Nyhan syndrome.¹⁶

One of the main challenges in the implementation of hiPSCs in clinical trials and scale-up manufacturing is cost, due to the growth factor requirements, especially for large-scale production. Thus, there is an urgent need to establish optimal and economically viable growth conditions to direct the differentiation of pluripotent stem cells in a defined nutritional microenvironment.

In addition to the economic issues, nutritional microenvironments can have an impact on cell type authenticity. Any perturbation in the energy metabolism could affect self-renewal, differentiation, and stem cell fate as the metabolism of pluripotent stem cells is different from their differentiated counterparts.^{17–20}

The analysis of the effects of the nutritional environment and energy metabolism on the differentiation of pluripotent stem cells (iPSCs and ESCs) *in vitro* is underpinned by the understanding of the embryo environment *in vivo*. During early development, the embryo is exposed to nutrients via vascular perfusion of the fallopian tube.^{21–23} The embryo resides in a low oxygen niche environment²⁴ and a switch from oxidative phosphorylation to glycolysis is sensed.²⁵ The embryo is exposed to low glucose concentration during early development,^{21–23} and it is known that the average oxygen levels in the human uterine surface change from 2.4% at Weeks 7–10 up to 7–8% after the maternal blood flows to the fetus in Week 11.²⁶ Thus, the *in vivo* concentrations of key nutrients that could have an effect on the metabolism such as oxygen, glucose, and pyruvate, are much lower than the *in vitro* differentiation conditions.^{21–24,27} In this study, the *in vivo* microenvironment was reproduced and compared to laboratory conditions and complete deprivation (0% oxygen, 0 mM glucose, 0 mM pyruvate).

To allow the investigation of three factors (oxygen, glucose, and pyruvate concentrations) with multiple concentrations in parallel, a design of experiments (DoE) approach was chosen to provide insights on the experimental space and interactions within factors.^{28,29}

The ability of DoE to generate an algorithmic model aids in the optimization of experimental conditions by highlighting any interaction that might exist between the factors while reducing the number of

experiments.^{28,29} DoE has been applied in fields such as engineering,^{30,31} drug optimization,^{32,33} microbiology,^{34,35} and in the optimization of the pluripotent stem cell media.³⁶ Nevertheless, to date, there are no studies that investigate the effect of nutritional microenvironment on germ layer formation using DoE. As a result, the aim of this study was to investigate whether mimicking the natural environment or depriving the oxygen, glucose, and pyruvate could enhance or affect germ layer formation.

2 | MATERIALS AND METHODS

2.1 | hiPSCs expansion and differentiation

Episomal hiPSC (Cord blood) line was purchased from Life Technologies (Lot number 1648638) and generated using cord blood-derived CD34+ progenitors with seven episomally expressed factors (OCT-4, SOX2, KLF4, c-MYC, NANOG, LIN28, and SV40 T). Mycoplasma testing was routinely performed and genetic instability of this cell line was assessed via karyotyping at Passages 40 and 63. This line was first grown on mouse feeders and then adapted to a feeder-free system. These cell lines were cultured in Essential 8 medium (Thermo-Fisher Scientific) on vitronectin VTN-N (Thermo-Fisher Scientific) coated flasks. The differentiation of hiPSCs was performed through single cell suspension differentiation. hiPSCs were washed with PBS before adding TrypLE (Gibco) and incubating for 5 min at 37°C, differentiation media was added, and cells were passed through a 40 µm cell strainer (BD Bioscience), then centrifuged at 1250 rpm for 5 min. After counting, cells were seeded as single cell in a 12-well plate precoated with reduced growth factor Matrigel (BD Bioscience) at a density of 0.8×10^5 cells/ml. Differentiation was induced by treating hiPSCs with DMEM-F12 (Gibco, catalogue number 11320033) and customized DMEM-F12 for other conditions. Customized media was produced, which did not contain glucose, pyruvate and glutamine. The media was supplemented with 20% knockout serum replacement media (Gibco), 1% Glutamax (Gibco), 1% nonessential amino acids (Gibco) and 0.1 β-mercaptoethanol (Gibco) and 1 ng/ml of Rho kinase inhibitor (Millipore). In conditions where cells were cultured at low oxygen tension, nitrogen was introduced into the incubators and sensors were used to confirm the desired oxygen tension. Additionally, media was primed at low oxygen levels before adding it to the differentiated cells. Cells were differentiated for 4 days in the different environmental conditions.

Biomarker	Description	QuantiTect primer assay	Catalogue number	Supplier
β-actin	Housekeeping gene	Hs_ACTB_2_SG	QT01680476	Qiagen
Tubulin 3	Ectodermal marker	Hs_TUBB3_1_SG	QT00083713	Qiagen
Nestin	Ectodermal marker	Hs_NES_2_SG	QT01015301	Qiagen
SOX17	Endodermal marker	Hs_SOX17_1_SG	QT00204099	Qiagen
FOXA2	Endodermal marker	Hs_FOXA2_1_SG	QT00212786	Qiagen
CXCR4	Endodermal marker	Hs_CXCR4_2_SG	QT02311841	Qiagen
Brachyury	Mesoderm marker	Hs_T_1_SG	QT00062314	Qiagen
KIFA	Mesoderm marker	Hs_KIF1A_1_SG	QT00072604	Qiagen

TABLE 1 Markers and primers used to evaluate the gene expression for germ layer formation and pluripotency

TABLE 2 Factors and levels used for the design of experiments

Factor	Level		
	Deprivation	Physiological environment	Laboratory conditions
Oxygen (% vol/vol)	0	2	20
Glucose (mM)	0	3.14	17.50
Pyruvate (mM)	0	0.14	0.50

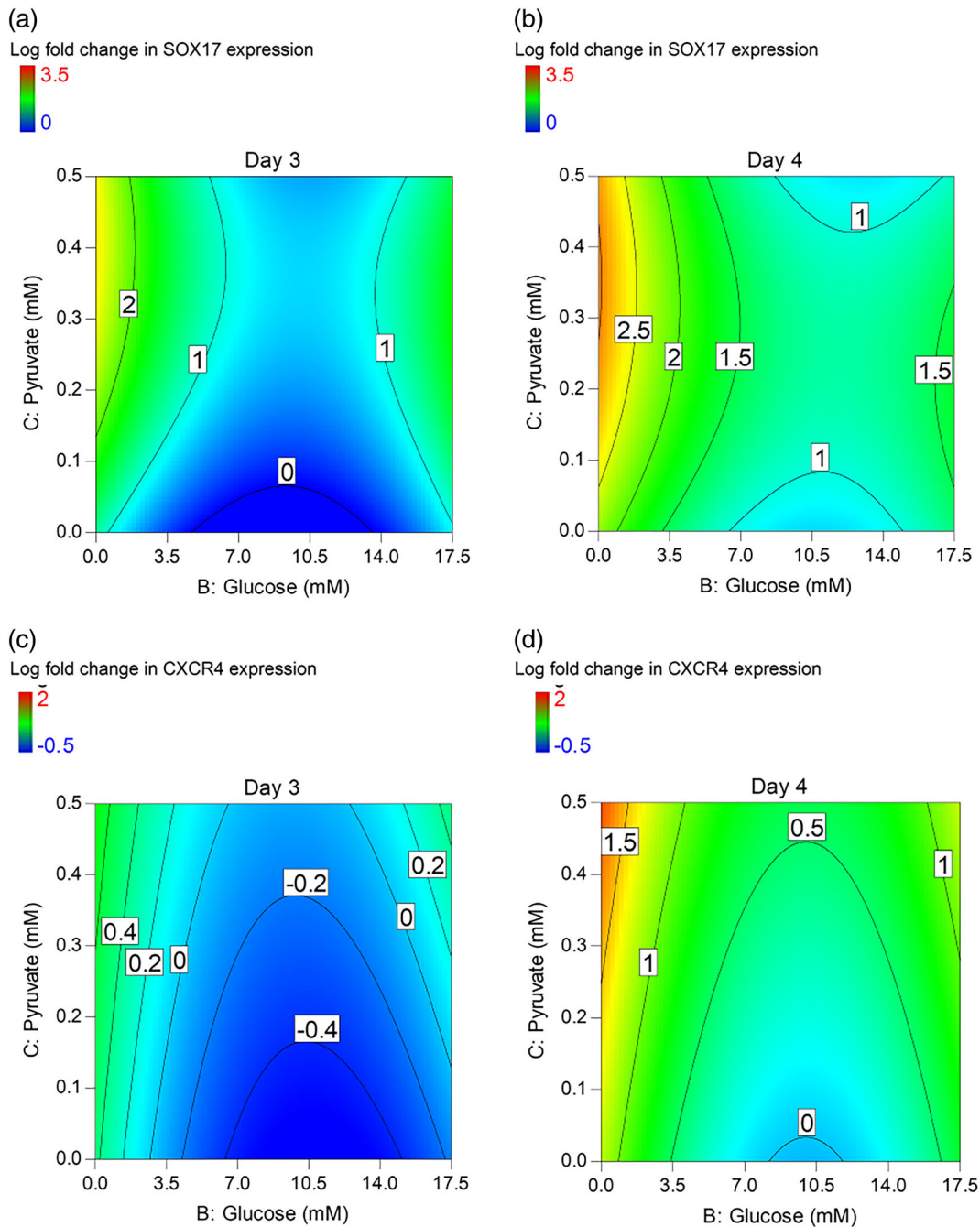


FIGURE 1 Contour maps of the model for endodermal gene expression at Days 3 and 4 after differentiation. Gene expression for differentiated induced pluripotent stem cells (iPSCs) was assessed by real-time polymerase chain reaction (RT-PCR). Colors ranging from dark blue to dark red represent the lowest and highest log value, respectively, for endodermal gene expression: (a) SOX 17 at Day 3, (b) SOX 17 at Day 4, (c) CXCR4 at Day 3, and (d) CXCR4 at Day 4

2.2 | Cell number quantification

Trypan blue exclusion method was used in order to assess cell numbers and viability. Cells were detached from the 12-well plate using TrypLE and run on a Vi-Cell counter (Beckman Coulter).

2.3 | Phase contrast microscopy for cell morphology

Phase contrast microscopy pictures of differentiated iPSCs derived from single cells in different conditions were taken using Evos XL (Thermo-Fisher Scientific) as an imaging system.

2.4 | Gene expression by real-time polymerase chain reaction

Gene expression after differentiation of hiPSCs was studied for endodermal markers (Sox17, FOXA2, and CXCR4), mesodermal markers (Brachyury and KIF1A), and ectodermal markers (Nestin, β -Tubulin) via real-time polymerase chain reaction (RT-PCR). First, RNA was extracted using RNeasy Micro Kit (Qiagen) as per manufacturer's instructions. At the end of the manufacturer's protocol, 40 μ l of RNA samples diluted in

RNAse-free water were obtained, and quantification was performed on a spectrophotometer (NanoDrop ND-1000, Thermo-Fisher Scientific) by measuring the absorbance at 260/280 nm. The synthesis of complementary deoxyribonucleic acid (cDNA) was then performed using a QuantiTect Reverse Transcription Kit (Qiagen) as per manufacturer's instructions. cDNA was obtained by first eliminating any genomic DNA contaminant by the addition of gDNA Wipeout buffer (Qiagen), which was added to up to 1 μ g of mRNA, then topped up to a final volume of 14 μ l with RNAse free water. The mixture was incubated at 42°C for 2 min in a thermocycler (Bio-Rad). Furthermore, a master mix of Primer Mix Quantiscript, RT buffer and Quantiscript Reverse Transcriptase were added to the template RNA (total volume of 20 μ l). The samples were run at 42°C for 15 min then at 95°C for 3 min and stored at -20°C. The cDNA synthesized from the previous step was mixed with Quantitect SYBR Green PCR Kits (Qiagen), Quantitect prevalidated primer assay, as shown in Table 1, and RNAse-free water to a total volume of 25 μ l, and then loaded in triplicate in Hard-Shell Low Profile Thin-Wall 96 Well Skirted PCR plates (Bio-Rad) and run on a Bio-Rad CFX 96 Connect Real-Time PCR machine for 40 cycles.

The PCR was performed screening for differentiation and pluripotent genes along with a housekeeping gene (β -actin). The C_t values were taken from the Bio-Rad CFX Manager 3.0 and fold changes were

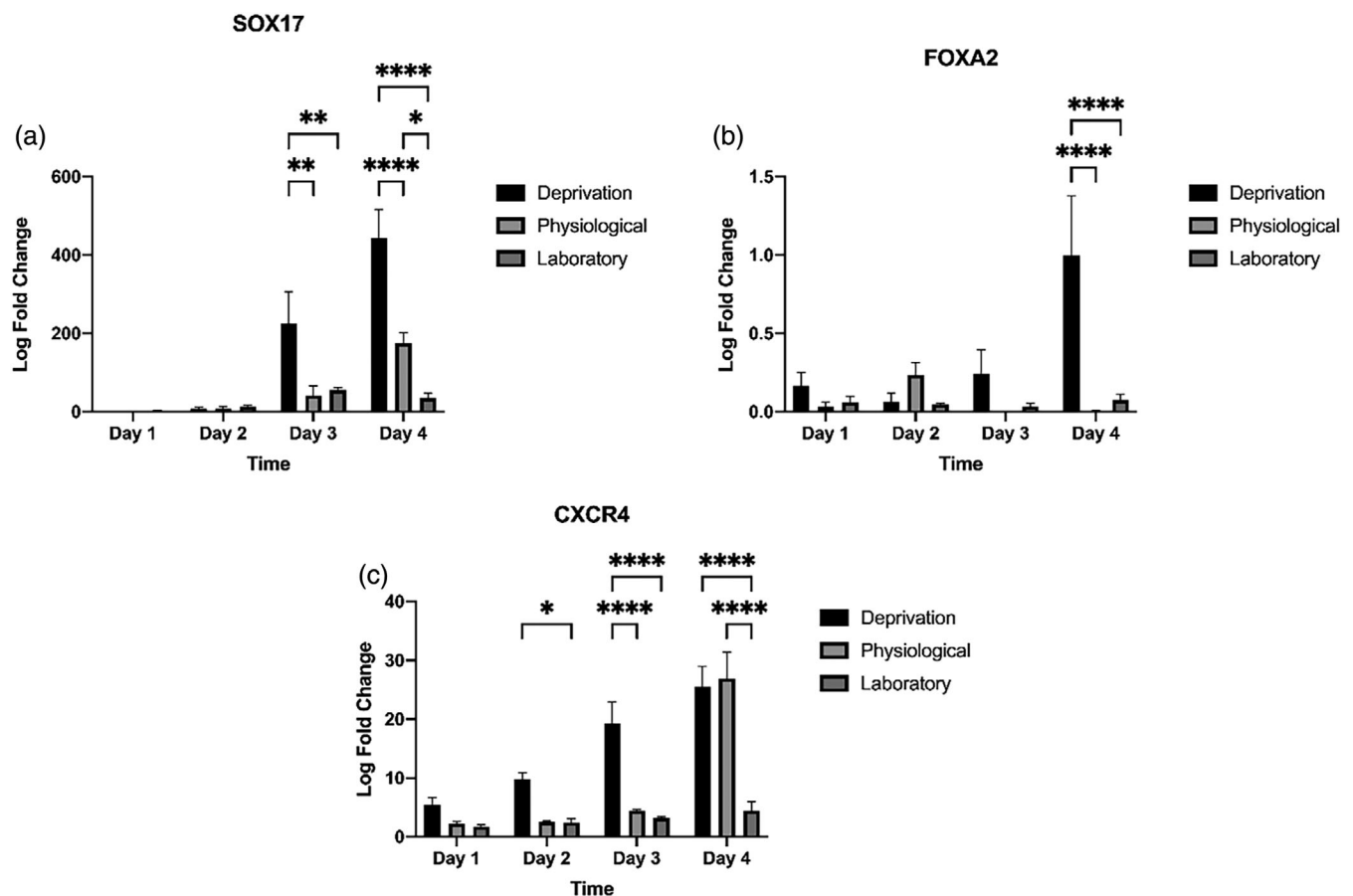


FIGURE 2 Endodermal gene expression for SOX17 (a), FOXA2 (b), and CXCR4 (c) over time at deprivation levels, physiological, and laboratory conditions. All real-time polymerase chain reaction (RT-PCR) data are shown as mean \pm SEM (N = 3)

calculated from the normalized relative expression ($\Delta\Delta C_t$) using Equation (1) (K. Livak).

$$\text{Fold change} = 2^{-\Delta\Delta C_t} \quad (1)$$

where $2^{-\Delta\Delta C_t} = \left[\frac{(C_t \text{ gene of interest} - C_t \text{ internal control})_{\text{sample A}}}{(C_t \text{ gene of interest} - C_t \text{ internal control})_{\text{sample B}}} \right]$.

2.5 | Design of experiments

To determine the optimal nutritional environment for each of the germ layers, a combination of the relative concentrations of glucose, pyruvate, and oxygen in laboratory, physiological, and deprivation environments (as shown in Table 2) was studied. A full factorial design comprising a set of 27 different conditions was generated in Design-Expert v10 DoE

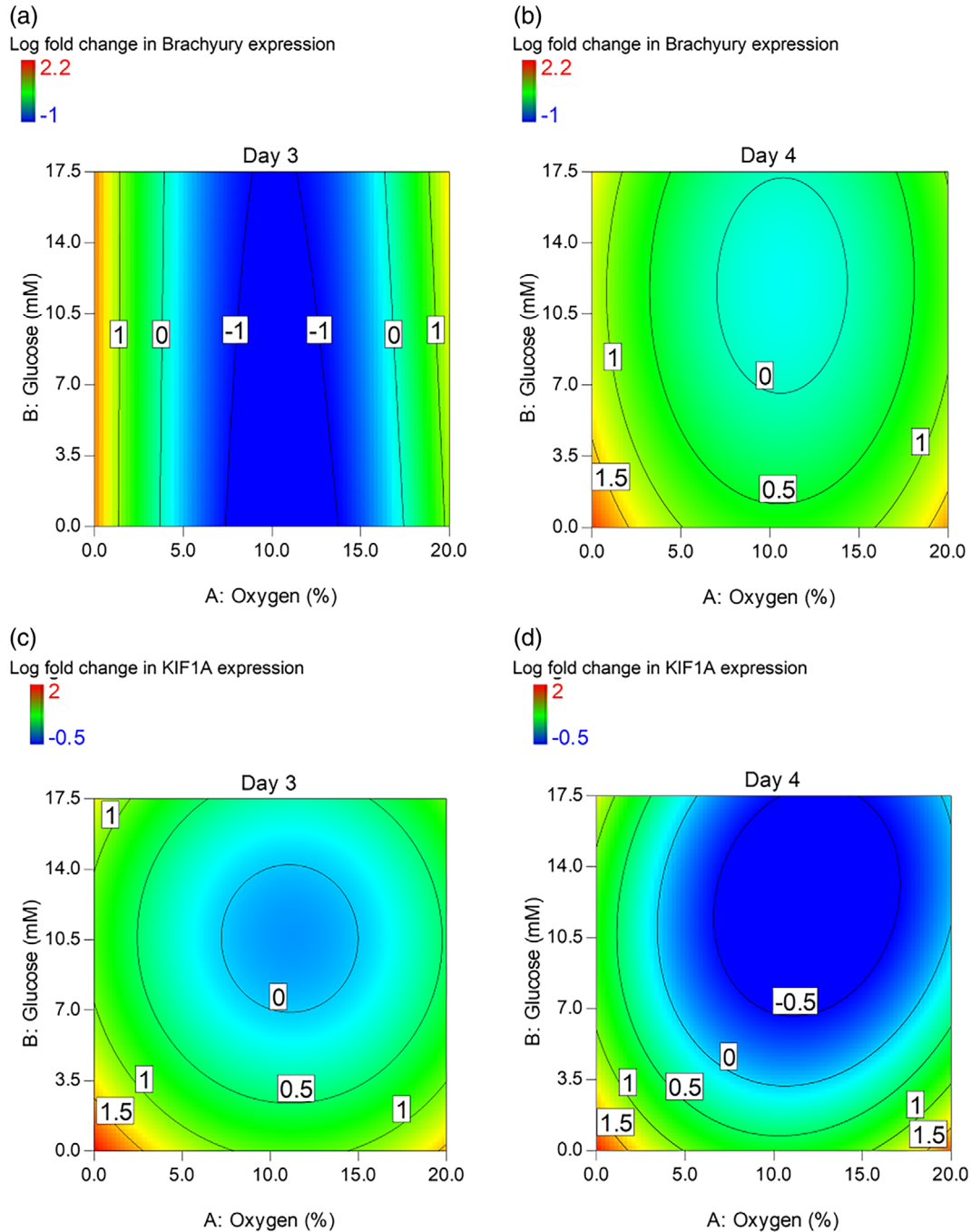


FIGURE 3 Contour maps of the model for mesodermal gene expression at Days 3 and 4 after differentiation. Gene expression for differentiated induced pluripotent stem cells (iPSCs) was assessed by real-time polymerase chain reaction (RT-PCR). Colors ranging from dark blue to dark red represent the lowest and highest log value, respectively, for endodermal gene expression: (a) Brachyury at Day 3, (b) Brachyury at Day 4, (c) KIF1A at Day 3, and (d) KIF1A at Day 4

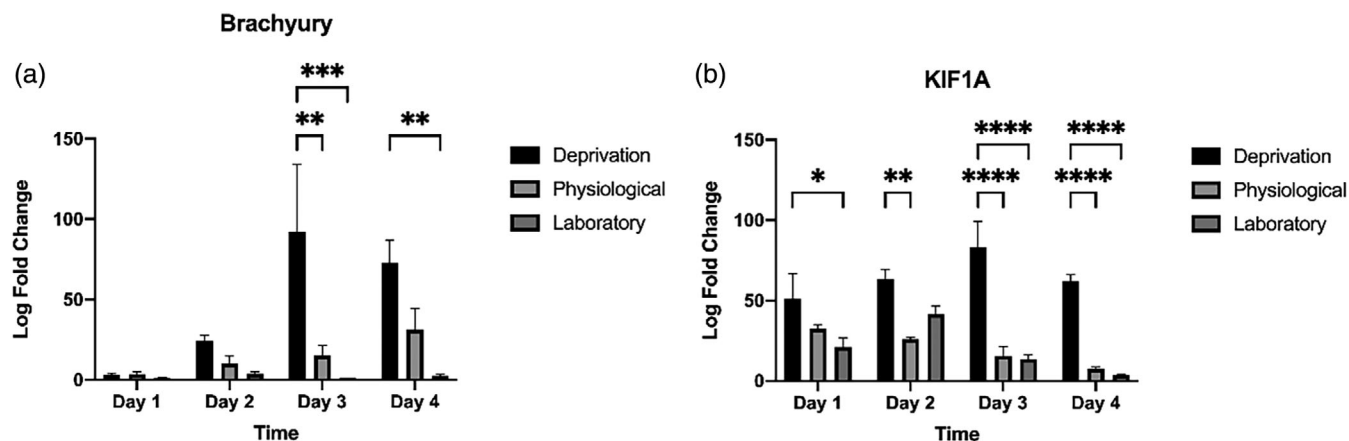


FIGURE 4 Mesodermal gene expression for Brachyury (a) and KIF1A (b) over time at deprivation levels, physiological, and laboratory conditions. All real-time polymerase chain reaction (RT-PCR) data are shown as mean \pm SEM ($N = 3$)

software (Stat-Ease, Inc., Minneapolis, MN) to allow the estimation of all possible interactions. The initial differentiation protocol was set for 7 days since the formation of in vivo germ layers occurs one week after gestation. As preliminary data (not shown) showed low viability in some conditions while expressing high gene expression, the differentiation time was shortened to 4 days. Glutamine levels were not measured as Glutamax was supplemented in the media because it is more stable than glutamine.

The 27 different combinations of the three factors (oxygen, pyruvate, and glucose concentrations) were tested for germ layer gene expression along with the cell counts. Differentiation of hiPSCs in each condition was performed in triplicate and the data generated from the RT-PCR during the 4 days of the differentiation process was fed back into the design software. Data for each response factor was transformed as appropriate in order to approximate a normal distribution, log fold gene expression was calculated to reduce the difference in the orders of magnitude between the expressions of different gene markers.³⁷ An automatic model selection tool was used to keep only significant terms in the model, as well as maximizing the resulting regression function of the model. The criterion used was backward p -value selection, set at a cut-off value of 0.1. ANOVA was used to analyze the reduced model to ensure statistical parameters were within the appropriate statistically significant limits. From the ANOVA analysis, F -values for all models were large enough to indicate adequate signal and reject the effect of noise. Overall, outputs from the ANOVA analysis suggested the models for all responses were significant. Using the gene expression for each of the germ layers and viable cell counts, a predictive mathematical model was generated to determine the best condition for the enhancement of each germ layer.

2.6 | Statistical analysis

The significance of the differences in the expression markers was tested using one-way ANOVA with Dunnett test and multiple comparisons for all conditions compared to the laboratory levels as control.

The significance of differences in the expression of genes over time at complete deprivation, physiological levels, and laboratory conditions was assessed using two-way ANOVA with multiple comparisons. Differences with p -values <0.05 are labeled with an asterisk (*); differences with p -values <0.001 are labeled with four asterisks (****).

3 | RESULTS AND DISCUSSION

3.1 | Glucose deprivation enhanced endodermal lineage formation

Monolayer single cell differentiated hiPSCs (cord blood) were cultured in 27 different conditions with varying levels of oxygen, glucose, and pyruvate concentrations as shown in Table 2. Design Expert v10 DoE software (Stat-Ease, Inc.) was used to analyze the response factors from this study. The software yielded significant models for SOX17 and CXCR4 at Days 3 and 4, thus FOXA2 was not presented in the contour maps shown in Figure 1. Oxygen was found to have no significant effect and was thus removed from the model by backward p -value elimination. The individual gene expression for all conditions was analyzed and compared to the laboratory levels as control using one-way ANOVA with Dunnett test and multiple comparisons for quantification (data not shown). Additionally, a detailed analysis using two-way ANOVA with multiple comparisons of the expression of endodermal genes over time at complete deprivation, physiological levels, and laboratory conditions can be seen in Figure 2 to account for time and concentration effects.

No significant differences were found in the expression of the early differentiation marker SOX17 or the late differentiation marker FOXA2 when compared to the control for any of the 27 conditions during the first day; however, the expression of CXCR4 was slightly higher at 0% oxygen tensions (data not shown). These findings are corroborated by the literature, and CXCR4 increased expression by hypoxia has previously been shown to be driven by hypoxia-inducible factor 1 (HIF-1 α).³⁸

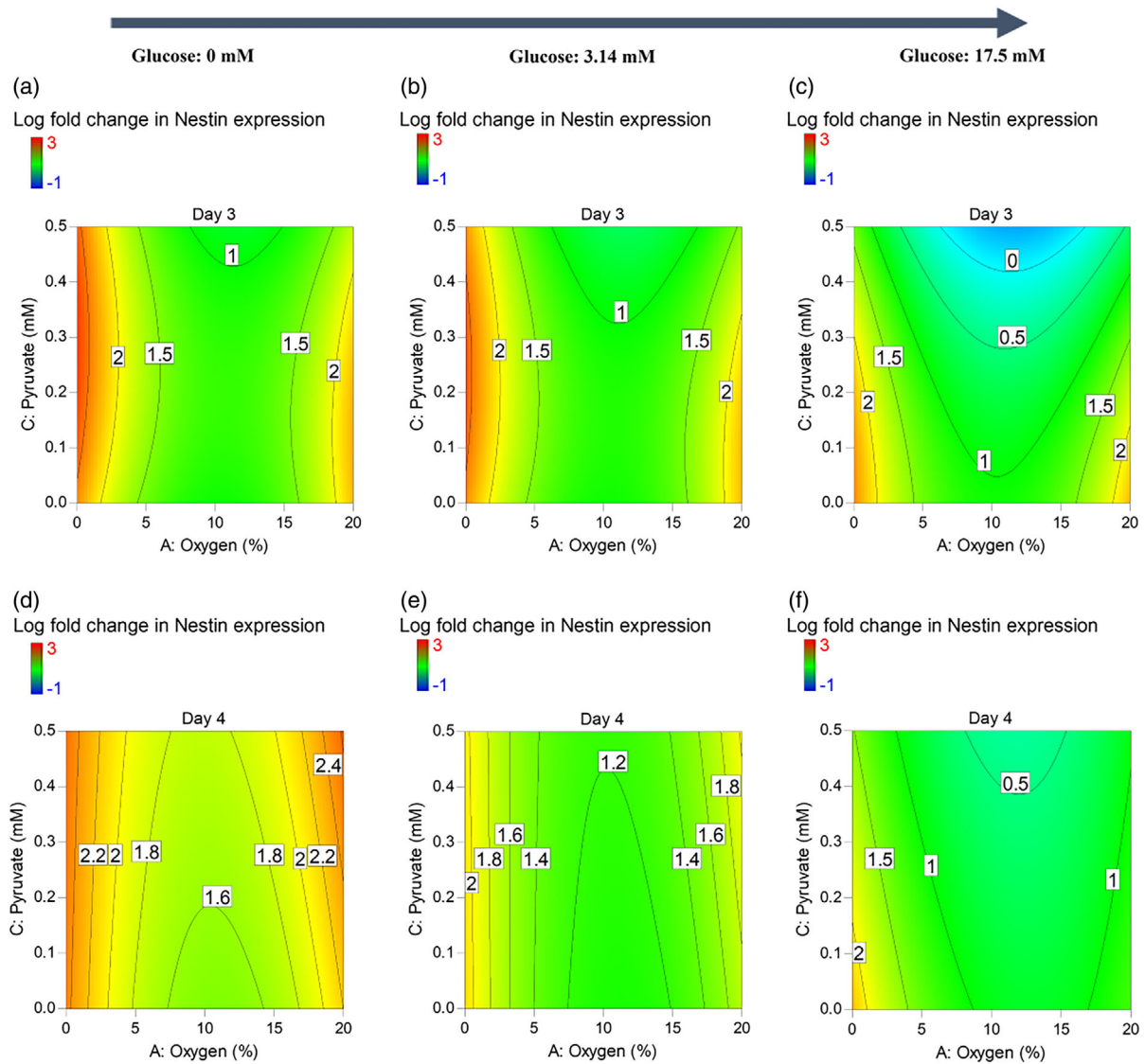


FIGURE 5 Contour maps of the model for Nestin gene expression at Days 3 (a–c) and 4 (d–f) after differentiation. Gene expression for differentiated induced pluripotent stem cells (iPSCs) was assessed by real-time polymerase chain reaction (RT-PCR). Colors ranging from dark blue to dark red represent the lowest and highest log value, respectively, for endodermal gene expression of Nestin

On Day 2, marginally higher SOX17 expression was seen when cells were exposed to deprived glucose media while maintaining the laboratory oxygen (20%) and pyruvate levels (0.14 mM) (Figure 2). This effect of glucose removal on SOX17 expression was seen clearly at Days 3 and 4 (Figure 2(c,d)), being significantly higher at complete depletion of glucose than both at physiological and laboratory levels at Day 3 (p -value = 0.0021 and 0.0041, respectively) and Day 4 (p -value <0.0001) as can be observed in Figure 2(a). The depletion of glucose induces downregulation of the pluripotency marker OCT4 via oxidation without causing apoptosis,³⁹ which is supported by our findings on cell viability (Figure 8). As a result of this reduction in OCT4 activity, endoderm-associated genes such as SOX17 are increasingly expressed.⁴⁰

The impact of complete deprivation on the expression of the late endodermal marker FOXA2 was seen on Day 3 and to a larger extent

on Day 4, as shown in Figure 2(b). It is reasonable to assume that, indeed, FOXA2 would be overexpressed in the absence of glucose, since this transcription factor is responsible for activating lipid metabolism and ketogenesis.⁴¹

Expression of CXCR4 was enhanced only at 20% O₂, 0 mM glucose; 0% O₂, 0 mM glucose, and 0% O₂, 17.50 mM glucose in the 4 days of differentiation (Figure 1(c,d)). Interestingly, the levels of CXCR4 in hiPSCs grown in physiological and deprivation conditions compared to their counterparts in the laboratory environment are consistently higher for all time points, yielding significant differences (p -value <0.0001) both at Days 3 and 4 (Figure 2(c)) due to the overexpression of HIF-1 α , which in turn stabilizes CXCR4 mRNA. This has been reported in various types of cancer niches.⁴²

Increasing the oxygen tension to 20% while keeping iPSCs deprived of glucose and under 0.14 mM pyruvate seems to increase

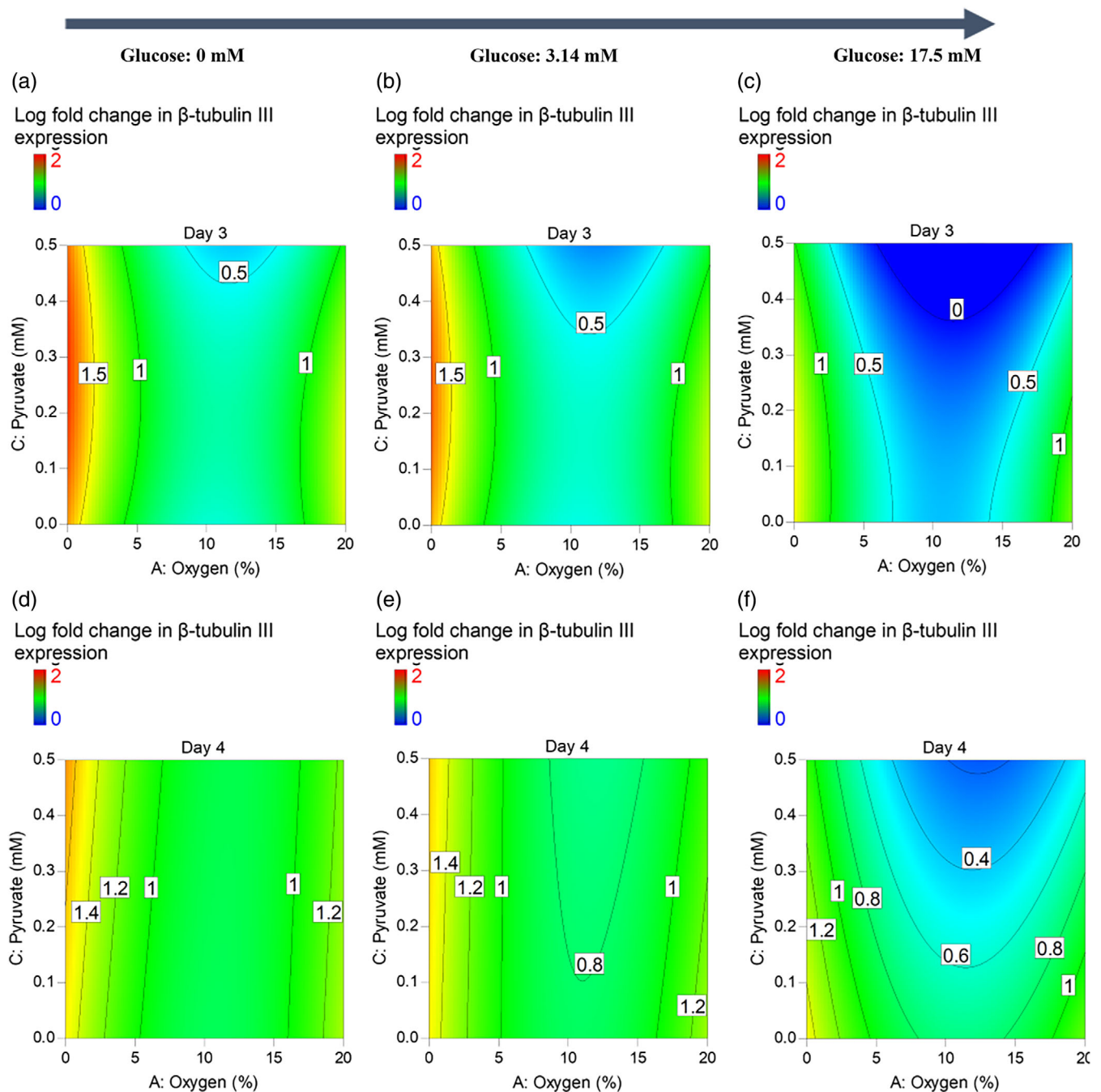


FIGURE 6 Contour maps of the model for Tubulin 3 gene expression at Days 3 (a–c) and 4 (d–f) after differentiation. Gene expression for differentiated induced pluripotent stem cells (iPSCs) was assessed by real-time polymerase chain reaction (RT-PCR). Colors ranging from dark blue to dark red represent the lowest and highest log value, respectively, for endodermal gene expression of Tubulin 3

the expression of endodermal markers even at Day 4 as seen in Figure 1(b,d) (1700-fold increase of Sox17, and 80-fold increase of CXCR4). This effect is more pronounced than when hiPSCs are exposed to the same conditions with higher pyruvate concentration (0.50 mM), since the presence of exogenous pyruvate potentiates the differentiation of stem cells toward mesodermal lineages.⁴³

Depleting glucose from media while keeping the physiological environmental levels of oxygen and pyruvate (2%, 0.14 mM,

respectively) enhances all endodermal markers from Day 2 onward (Figures 1 and 2). The deprivation of all three factors induced endodermal expression with a maximum of ~500-fold increase of SOX17 and ~40-fold increase of CXCR4 at Day 3 without inducing the definitive endodermal marker (FOXA2) (Figure 2). We found that culturing hiPSCs in glucose-deprived media enhanced the endodermal gene expression while maintaining normal oxygen and pyruvate levels. Previous studies reported that low glucose

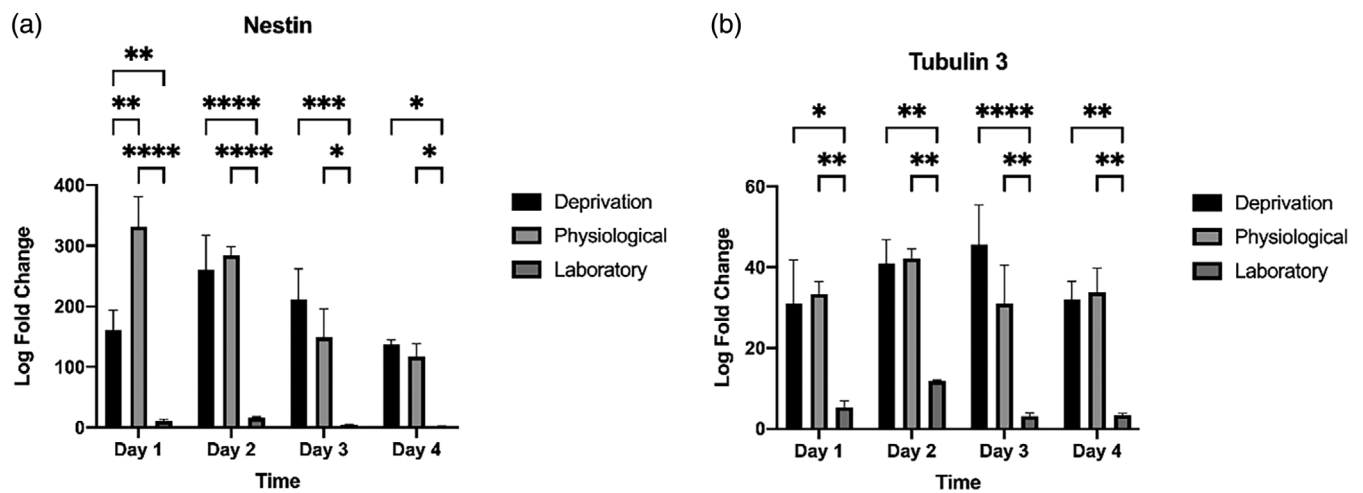


FIGURE 7 Ectodermal gene expression for Nestin (a) and Tubulin 3 (b) over time at deprivation levels, physiological, and laboratory conditions. All real-time polymerase chain reaction (RT-PCR) data are shown as mean \pm SEM ($N = 3$)

has been shown to stimulate the commitment of human hematopoietic stem cells to the erythroid lineage⁴⁴ and maturation of mesenchymal stem cells (MSCs).⁴⁵

There are several studies that focus on the effect of glucose concentration on the proliferation of mouse embryonic stem cells (mESCs),⁴⁶ human bone marrow-derived MSC,⁴⁷ human hematopoietic stem cell differentiation,⁴⁴ and MSCs,^{48,49} yet, to date, there is no evidence of the combined effect of oxygen, glucose, and pyruvate and their interaction on germ layer formation without the addition of growth factors in the differentiation media.

3.2 | Mesodermal differentiation was enhanced at low oxygen and glucose levels

Deprivation or exposing the cells to pyruvate did not have a significant effect on the mesodermal gene expression (Brachyury and KIF1A) during the 4 days of differentiation; thus, pyruvate was removed from the model by backward p -value elimination. Expression of Brachyury was increased only on the edges of the contouring area²⁹ as seen in Figure 3(d), when the oxygen was the lowest or the highest. Further quantification in Figure 4(a) shows that Brachyury was overexpressed both in deprivation and physiological conditions as opposed to laboratory conditions. The expression of KIF1A was increased with lower oxygen tensions at all time points (Figure 4(b)). Moreover, glucose depleted media had an effect on the expression of KIF1A compared to laboratory and physiological conditions, particularly on Day 4 as demonstrated on Figure 4(b) (p -value < 0.0001). Lower oxygen tension (0–2%) somehow enhanced the expression of Brachyury and KIF1A in the 4 days of differentiation (Figure 3(d)). The contour area for mesodermal expression generally did not show noticeable differences in the gene expression for the

27 conditions at Days 1 and 2 (data not shown), but clearly defined optimal conditions were observed at Days 3 and 4 (Figure 3), with high expression of both markers at low oxygen tension. The combined effect of lower oxygen and glucose levels for the enhancement of mesodermal lineages is demonstrated in Figure 4. During differentiation, higher concentrations of pyruvate direct mesoderm and endoderm lineage specification, mainly in oxygen and glucose-deprived environments as seen in Figures 1 and 3, which is supported by the literature.⁴³

3.3 | High oxygen levels decreased ectodermal gene expression

An analogous analysis was performed for ectodermal gene expression, and a quadratic model was fitted for ectodermal markers. The contour plots and analysis of gene expression over time at complete deprivation of glucose and pyruvate, physiological levels of these components and laboratory concentrations can be seen in Figures 5 and 6 respectively. As the pyruvate concentration was increased from 0 to 0.50 mM, the expression of ectodermal markers (Nestin and Tubulin 3) did not change when the cells were exposed to 0 mM glucose (Figures 5 and 6). Moreover, the expression of Tubulin 3 was higher when hiPSCs were cultured at low oxygen tension (0%) during the 4 days. The general observed pattern in the ectodermal expression was that upon increasing the glucose and oxygen levels, the level of expression of Nestin and Tubulin 3 decreased—this can be observed in Figure 7, where for all time points the expression of both markers was significantly higher to various degrees at deprivation and physiological conditions, where the concentrations are lower than in the laboratory environment. Differentiating hiPSCs at 0% O₂ and 0 mM glucose also induced ectodermal markers with a maximum gene expression at Day 3 (Figure 5–7).

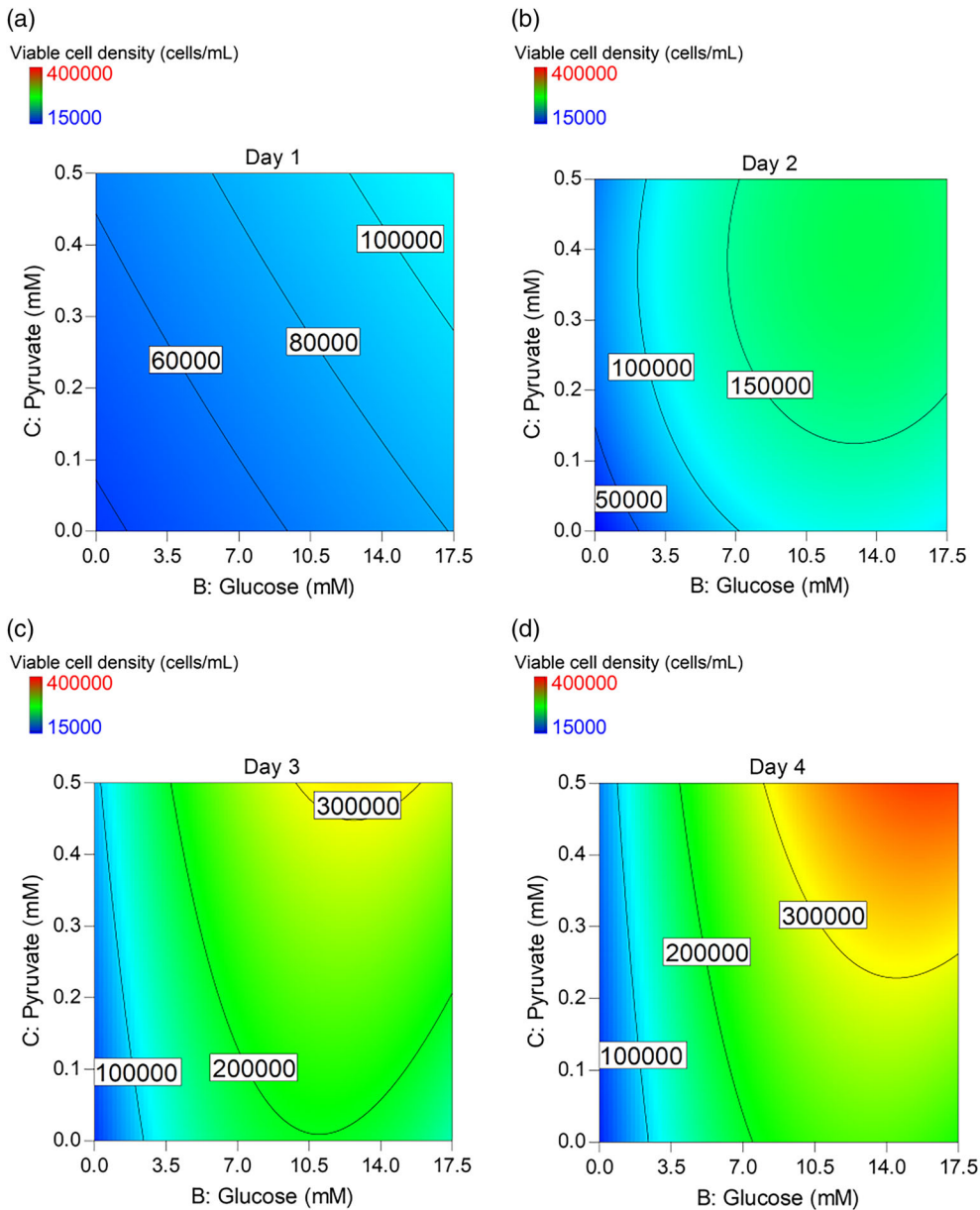


FIGURE 8 Contour maps of the model for viable cell density of the 27 conditions within the 4 days of differentiation. Cell viability was assessed via the trypan blue exclusion method. Colors ranging from dark blue to dark red represent the lowest and highest value for viable cell count, respectively, at Day 1 (a), Day 2 (b), Day 3 (c), and Day 4 (d)

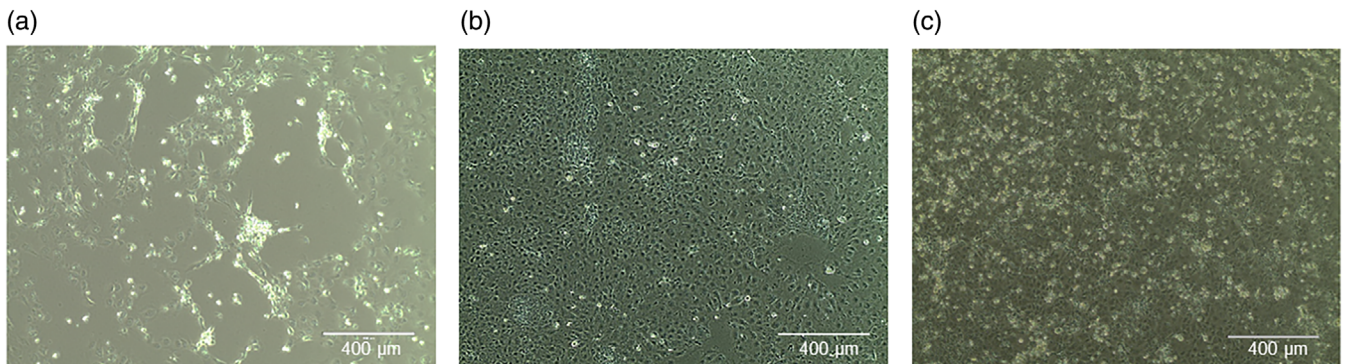


FIGURE 9 Bright-field micrographs of induced pluripotent stem cells (iPSCs) cultured at deprivation levels (a), physiological (b), and laboratory (c) conditions after 4 days of differentiation. Images were taken at $\times 100$ ocular magnification using Evos XL. Scale bars = 400 μm

TABLE 3 Culture conditions informed by the predictive model to direct differentiation toward a particular lineage via manipulation of oxygen, glucose, and pyruvate concentrations

Germ layer	Oxygen (%)	Glucose (mM)	Pyruvate (mM)	Desirability
Endoderm	20	0.10	0.5	0.61
Mesoderm	0	0.15	0.5	0.75
Ectoderm	0	1.00	0.5	0.78

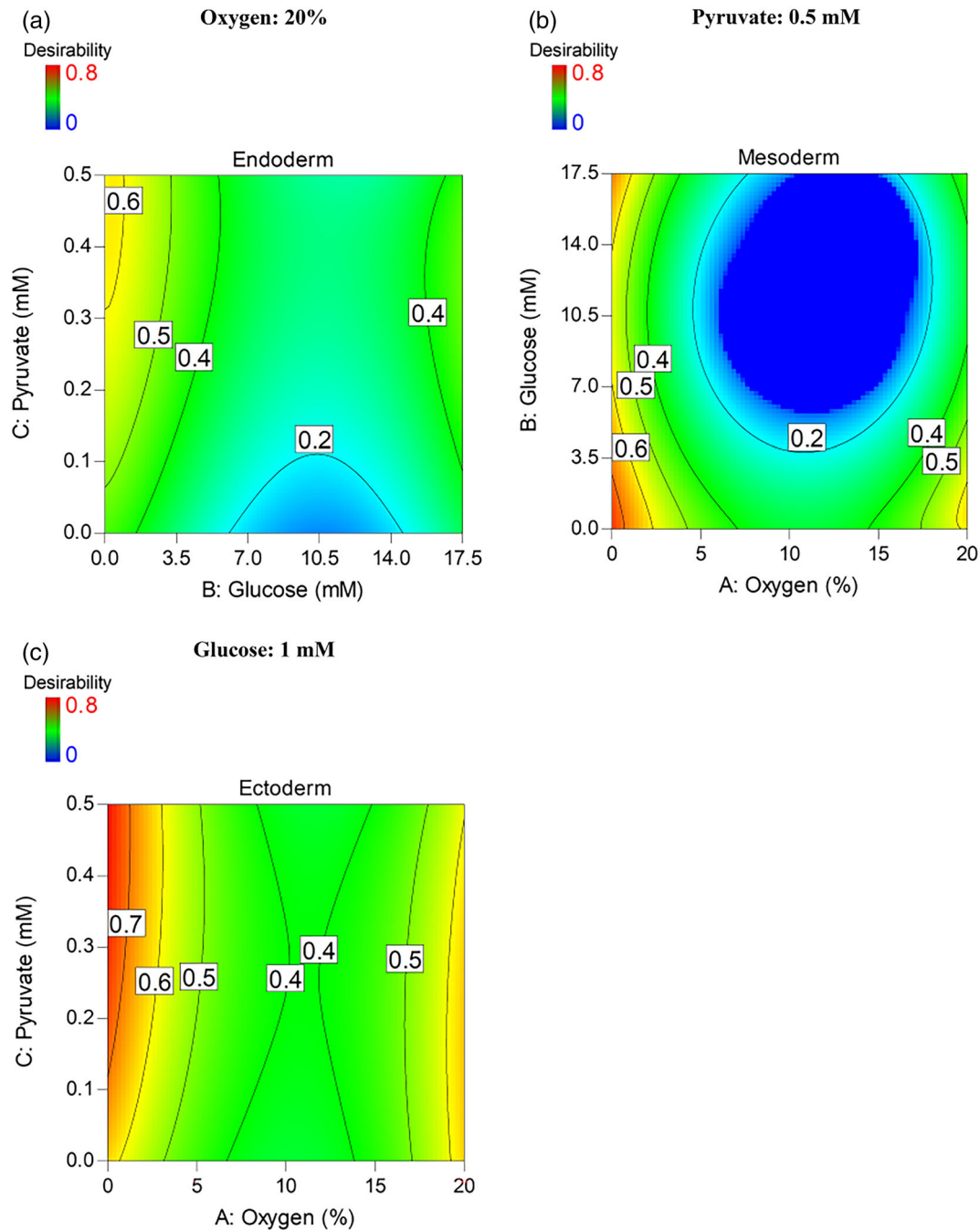


FIGURE 10 Predictive model for maximum gene expression and cell viability in each germ layer. Colors ranging from dark blue (0) to dark red (1) represent the lowest and highest values for desirability. The dashed area in each model represents the optimum range predicted by the model for endoderm (a), mesoderm (b), and ectoderm (c) germ layers

We found that oxygen and glucose deprivation enhanced the ectodermal and mesodermal germ layer formation from the second day after the start of the differentiation process. The effect of oxygen

deprivation alone has been shown in the literature for differentiated human ESCs or mESCs, where lower oxygen tension stimulated the formation of mesoderm⁵⁰⁻⁵² and ectodermal precursors.^{53,54}

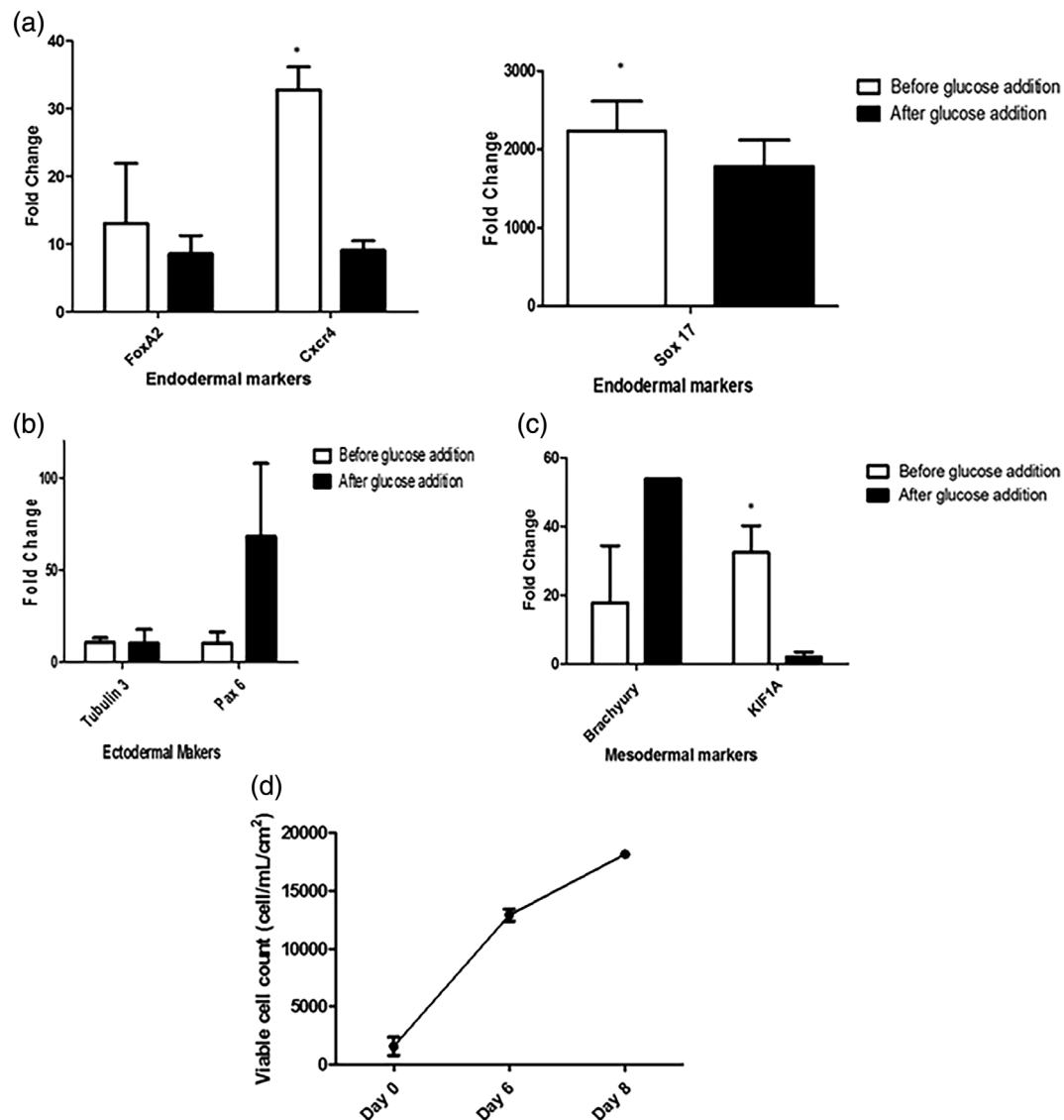


FIGURE 11 Adding glucose to the media retained the endodermal lineage expression of differentiated human episomal induced pluripotent stem cells (iPSCs) (Cord blood). Real-time polymerase chain reaction (PCR) was performed in order to assess the fold gene expression of each germ layer: (a) Endoderm (Sox 17, FOXA2, CXCR4), (b) ectoderm (Nestin, Tubulin 3, Pax6), and (c) mesoderm (Brachyury, KIF1A) for normal and deprived conditions. (d) cell viability was assessed by trypan blue exclusion method

3.4 | The effect of glucose and oxygen levels on cell viability and cell morphology

Cell viability of hiPSCs was assessed via trypan blue exclusion method and is reported as a function of oxygen, glucose, and pyruvate levels over time in Figure 8. Culturing hiPSCs in laboratory conditions led to the highest cell counts for all time points. As expected, stressing hiPSCs through exposure to deprived glucose and oxygen environments had an impact on cell viability.⁵⁵ Although higher gene expression was observed in some extreme conditions for each germ layer, lower viabilities were found. In general, low pyruvate concentrations (<0.14 mM) promoted higher cell viability regardless of the concentration of glucose. For all levels of oxygen, reducing the concentration of glucose had a negative

effect on viable cell counts. Despite subjecting hiPSCs to various conditions, including extreme deprivation of nutrients and oxygen, the morphology of the cells was found to be normal and healthy in appearance as shown in Figure 9.

3.5 | Germ layer optimization and model predictability

For each germ layer, the numerical optimization tool in Design Expert was used to find the optimal set of conditions that maximized both gene expression and viable cell density. The numerical optimization tool combines the desired goal of several response factors into an overall model desirability, which ranges from zero to one

(with 1 having the highest desirability), thus the best condition retrieved from the model should have the highest model desirability.

The optimal set of conditions that achieved the highest desirability for each germ layer are summarized in Table 3. The output from the optimization is also illustrated graphically in Figure 10. In summary, the enhancement of endodermal lineage gene expression occurred at low glucose levels, while low oxygen and glucose enhanced the mesodermal and ectodermal gene expression.

3.6 | The effect of glucose addition on the predictive endoderm model

To test the optimized condition generated by the predictive model for endodermal lineage (Table 3), cells were cultured in 0.10 mM glucose media while maintaining laboratory conditions for oxygen and pyruvate (20% and 0.5 mM respectively). Furthermore, to establish whether glucose-deprived cells could proliferate and retain their high endodermal gene expression after the 3-day starvation period, media containing glucose was added to maintain the cells from Day 4 onward. The glucose-deprived cells were able to proliferate and maintain high endodermal gene expression even 23 days post-starvation (Figure 11(d)). The endodermal gene expression of Sox 17 and CXCR4 decreased significantly after the glucose addition while the expression of FOXA2 remained unchanged (Figure 11(a)). While there was no significant change in the ectodermal (Tubulin and Pax6) and mesodermal (Brachyury and KIFIA) expression as seen in Figure 11(b,c). The addition of glucose helped in the proliferation of the differentiated cells while maintaining its phenotype.

4 | CONCLUSION

Despite technological advances, there are still numerous challenges in the production of large quantities of clinical grade iPSCs for cell therapies. The differentiation process into any lineage is hindered by several bioprocess challenges, both upstream and downstream. If differentiation at scale is desired, high costs associated with the need for growth factors and other media components make manufacturing processes unaffordable. Optimizing differentiation is therefore a key step in scaling-up, and this can be achieved by applying the existing in-depth understanding of early differentiation of the embryo in vivo. During early embryo development, the levels of oxygen and metabolites are lower than in laboratory conditions; thus, the initial aim of this study was to investigate the impact of oxygen and nutrients on hiPSC proliferation and differentiation. We found that glucose deprivation enhanced endodermal lineage formation, particularly at physiological levels of oxygen and pyruvate. Mesodermal and ectodermal differentiations were enhanced in oxygen and glucose-deprived environments. These results informed our predictive model, which provides a novel approach for the efficient and cost-effective directed differentiation of iPSCs. Validation of the model and modification of simple growth parameters can allow the achievement of optimal

differentiation pathways, providing the basis for a potential scale-up platform where differentiation is merely directed by varying concentrations of glucose, oxygen, and pyruvate in the media.

ACKNOWLEDGMENT

The authors would like to acknowledge UCL's Department of Biochemical Engineering and IDB for funding this project.

CONFLICT OF INTEREST

The authors declare no conflict of interest.

PEER REVIEW

The peer review history for this article is available at <https://publons.com/publon/10.1002/btpr.3143>.

DATA AVAILABILITY STATEMENT

Data available on request from the authors.

ORCID

Rana Khalife  <https://orcid.org/0000-0001-7956-9707>

REFERENCES

- Meyer JR. The significance of induced pluripotent stem cells for basic research and clinical therapy. *J Med Ethics*. 2008;34(12):849-851. <https://doi.org/10.1136/jme.2008.024786>.
- Robinton DA, Daley GQ. The promise of induced pluripotent stem cells in research and therapy. *Nature*. 2012;481(7381):295-305. <https://doi.org/10.1038/nature10761>.
- Takahashi K, Yamanaka S. Induction of pluripotent stem cells from mouse embryonic and adult fibroblast cultures by defined factors. *Cell*. 2006;126:663-676. <https://doi.org/10.1016/j.cell.2006.07.024>.
- Takahashi K, Tanabe K, Ohnuki M, et al. Induction of pluripotent stem cells from adult human fibroblasts by defined factors. *Cell*. 2007;107(5):861-872. <https://doi.org/10.1016/j.cell.2007.11.019>.
- Kriks S, Shim JW, Piao J, et al. Dopamine neurons derived from human ES cells efficiently engraft in animal models of Parkinson's disease. *Nature*. 2011;480:547-551. <https://doi.org/10.1038/nature10648>.
- Wernig M, Zhao JP, Pruszak J, et al. Neurons derived from reprogrammed fibroblasts functionally integrate into the fetal brain and improve symptoms of rats with Parkinson's disease. *Proc Natl Acad Sci U S A*. 2008;105(15):5856-5861. <https://doi.org/10.1073/pnas.0801677105>.
- Nori S, Okada Y, Yasuda A, et al. Grafted human-induced pluripotent stem-cell-derived neurospheres promote motor functional recovery after spinal cord injury in mice. *Proc Natl Acad Sci U S A*. 2011;108(40):16825-16830. <https://doi.org/10.1073/pnas.1108077108>.
- Tsuji O, Miura K, Okada Y, et al. Therapeutic potential of appropriately evaluated safe-induced pluripotent stem cells for spinal cord injury. *Proc Natl Acad Sci U S A*. 2010;107(28):12704-12709. <https://doi.org/10.1073/pnas.0910106107>.
- Takayama N, Nishimura S, Nakamura S, et al. Transient activation of c-MYC expression is critical for efficient platelet generation from human induced pluripotent stem cells. *J Exp Med*. 2010;207(13):2817-2830. <https://doi.org/10.1084/jem.20100844>.
- Okamoto S, Takahashi M. Induction of retinal pigment epithelial cells from monkey iPS cells. *Invest Ophthalmol Vis Sci*. 2011;52(12):8785-8790. <https://doi.org/10.1167/iovs.11-8129>.
- Dimos JT, Rodolfa KT, Niakan KK, et al. Induced pluripotent stem cells generated from patients with ALS can be differentiated into

- motor neurons. *Science*. 2008;321(5893):1218-1221. <https://doi.org/10.1126/science.1158799>.
12. Devine MJ, Ryten M, Vodicka P, et al. Parkinson's disease induced pluripotent stem cells with triplication of the α -synuclein locus. *Nat Commun*. 2011;2(1):440. <https://doi.org/10.1038/ncomms1453>.
 13. Yagi T, Ito D, Okada Y, et al. Modeling familial Alzheimer's disease with induced pluripotent stem cells. *Hum Mol Genet*. 2011;20(23):4530-4539. <https://doi.org/10.1093/hmg/ddr394>.
 14. Yahata N, Asai M, Kitaoka S, et al. Anti-A β drug screening platform using human iPS cell-derived neurons for the treatment of Alzheimer's disease. *PLoS One*. 2011;6(9):e25788. <https://doi.org/10.1371/journal.pone.0025788>.
 15. Brennand KJ, Simone A, Jou J, et al. Modelling schizophrenia using human induced pluripotent stem cells. *Nature*. 2011;473(7346):221-225. <https://doi.org/10.1038/nature09915>.
 16. Park IH, Arora N, Huo H, et al. Disease-specific induced pluripotent stem cells. *Cell*. 2008;134(5):877-886. <https://doi.org/10.1016/j.cell.2008.07.041>.
 17. Kondoh H, Leonart ME, Nakashima Y, et al. A high glycolytic flux supports the proliferative potential of murine embryonic stem cells. *Antioxid Redox Signal*. 2007;9(3):293-299. <https://doi.org/10.1089/ars.2006.1467>.
 18. Sperber H, Mathieu J, Wang Y, et al. The metabolome regulates the epigenetic landscape during naive-to-primed human embryonic stem cell transition. *Nat Cell Biol*. 2015;17(12):1523-1535. <https://doi.org/10.1038/ncb3264>.
 19. Varum S, Rodrigues AS, Moura MB, et al. Energy metabolism in human pluripotent stem cells and their differentiated counterparts. *PLoS One*. 2011;6(6):e20914. <https://doi.org/10.1371/journal.pone.0020914>.
 20. Vernardis SI, Terzoudis K, Panoskaltis N, Mantalaris A. Human embryonic and induced pluripotent stem cells maintain phenotype but alter their metabolism after exposure to ROCK inhibitor. *Sci Rep*. 2017;7:42138-42149. <https://doi.org/10.1038/srep42138>.
 21. Dickens CJ, Maguiness SD, Comer MT, Palmer A, Rutherford AJ, Leese HJ. Physiology: human tubal fluid: formation and composition during vascular perfusion of the fallopian tube. *Hum Reprod*. 1995;10(3):505-508. <https://doi.org/10.1093/oxfordjournals.humrep.a135978>.
 22. Gardner DK, Lane M, Calderon I, Leeton J. Environment of the preimplantation human embryo in vivo: metabolite analysis of oviduct and uterine fluids and metabolism of cumulus cells. *Fertil Steril*. 1996;65(2):349-353. [https://doi.org/10.1016/S0015-0282\(16\)58097-2](https://doi.org/10.1016/S0015-0282(16)58097-2).
 23. Tay JI, Rutherford AJ, Killick SR, Maguiness SD, Partridge RJ, Leese HJ. Human tubal fluid: production, nutrient composition and response to adrenergic agents. *Human Reprod*. 1997;12(11):2451-2456. <https://doi.org/10.1093/humrep/12.11.2451>.
 24. Fischer B, Bavister BD. Oxygen tension in the oviduct and uterus of rhesus monkeys, hamsters and rabbits. *J Reprod Fertil*. 1993;99:673-679. <https://doi.org/10.1530/jrf.0.0990673>.
 25. Leese HJ, Barton AM. Pyruvate and glucose uptake preimplantation embryos. *J Reprod Fertil*. 1984;72:9-13. <https://doi.org/10.1530/jrf.0.0720009>.
 26. Rodesch F, Simon P, Donner C, Jauniaux E. Oxygen measurements in endometrial and trophoblastic tissues during early pregnancy. *Obstet Gynecol*. 1992 Aug;80(2):283-5. PMID: 1635745.
 27. Yang H, Qiu Y, Zeng X, et al. Effect of a feeder layer composed of mouse embryonic and human foreskin fibroblasts on the proliferation of human embryonic stem cells. *Exp Ther Med*. 2016;11(6):2321-2328. <https://doi.org/10.3892/etm.2016.3204>.
 28. Lundstedt T, Seifert E, Abramo L, et al. Experimental design and optimization. *Chemom Intel Lab Syst*. 1998;42:3-40. [https://doi.org/10.1016/S0169-7439\(98\)00065-3](https://doi.org/10.1016/S0169-7439(98)00065-3).
 29. Montgomery DC. *Design and Analysis of Experiments*. 8th ed.; John Wiley & Sons; 2012;1:752.
 30. Ariffin M et al. An optimise drilling process for an aircraft composite structure using design of experiments. *Sci Res Essays*. 2009;4(10):1109-1116.
 31. Thielman J, Ge P. Applying axiomatic design theory to the evaluation and optimization of large-scale engineering systems. *J Eng Des*. 2006;17(1):1-16. <https://doi.org/10.1080/09544820500287722>.
 32. Martinello T, Kaneko TM, Velasco MVR, Taqueda MES, Consiglieri VO. Optimization of poorly compactable drug tablets manufactured by direct compression using the mixture experimental design. *Int J Pharm*. 2006;322(1-2):87-95. <https://doi.org/10.1016/j.ijpharm.2006.05.034>.
 33. Singh B, Dahiya M, Saharan V, Ahuja N. Optimizing drug delivery systems using systematic "design of experiments." Part II: retrospect and prospects. *Crit Rev Ther Drug Carrier Syst*. 2005;22(3):215-294. <https://doi.org/10.1615/CritRevTherDrugCarrierSyst.v22.i3.10>.
 34. Esteban PP, Alves DR, Enright MC, et al. Enhancement of the antimicrobial properties of bacteriophage-K via stabilization using oil-in-water nano-emulsions. *Biotechnol Prog*. 2014;30(4):932-944. <https://doi.org/10.1002/btpr.1898>.
 35. Mannall GJ, Titchener-Hooker NJ, Dalby PA. Factors affecting protein refolding yields in a fed-batch and batch-refolding system. *Biotechnol Bioeng*. 2007;97(6):1523-1534. <https://doi.org/10.1002/bit.21377>.
 36. Marinho PA, Chailangkarn T, Muotri AR. Systematic optimization of human pluripotent stem cells media using Design of Experiments. *Sci Rep*. 2015;5:9834-9847. <https://doi.org/10.1038/srep09834>.
 37. Guy HM, McCloskey L, Lye GJ, Mitrophanous KA, Mukhopadhyay TK. Characterization of lentiviral vector production using microwell suspension cultures of HEK293T-derived producer cells. *Human Gene Therapy Methods*. 2013;24(2):125-139. <https://doi.org/10.1089/hgtb.2012.200>.
 38. Staller P, Sulitkova J, Lisztwan J, Moch H, Oakeley EJ, Krek W. Chemokine receptor CXCR4 downregulated by von Hippel-Lindau tumour suppressor pVHL. *Nature*. 2003;425:307-311.
 39. Marsboom G, Zhang GF, Pohl-Avila N, et al. Glutamine metabolism regulates the pluripotency transcription factor OCT4. *Cell Rep*. 2016;16(2):323-332.
 40. Hay DC, Sutherland L, Clark J, Burton T. Oct-4 knockdown induces similar patterns of endoderm and trophoblast differentiation markers in human and mouse embryonic stem cells. *Stem Cells*. 2004;22:225-235.
 41. von Meyenn F, Porstmann T, Gasser E, et al. Glucagon-induced acetylation of Foxa2 regulates hepatic lipid metabolism. *Cell Metab*. 2013;17:436-447.
 42. Guo M, Cai C, Zhao G, et al. Hypoxia promotes migration and induces CXCR4 expression via HIF-1 α activation in human osteosarcoma. *PLoS One*. 2014;9(3):e90518.
 43. Song C, Xu F, Ren Z, et al. Elevated exogenous pyruvate potentiates mesodermal differentiation through metabolic modulation and AMPK/mTOR pathway in human embryonic stem cells. *Stem Cell Rep*. 2019;13(2):338-351. <https://doi.org/10.1016/j.stemcr.2019.06.003>.
 44. Oburoglu L, Tardito S, Fritz V, et al. Glucose and glutamine metabolism regulate human hematopoietic stem cell lineage specification. *Cell Stem Cell*. 2014;15(2):169-184. <https://doi.org/10.1016/j.stem.2014.06.002>.
 45. Farrell MJ, Shin JI, Smith LJ, Mauck RL. Functional consequences of glucose and oxygen deprivation on engineered mesenchymal stem cell-based cartilage constructs. *Osteoarthr Cartil*. 2015;23(1):134-142. <https://doi.org/10.1016/j.joca.2014.09.012>. FUNCTIONAL.
 46. Kim YH, Heo JS, Han HJ. High glucose increase cell cycle regulatory proteins level of mouse embryonic stem cells via PI3-K/Akt and MAPKs signal pathways. *J Cell Physiol*. 2006;209(1):94-102. <https://doi.org/10.1002/jcp.20706>.
 47. Li YM, Schilling T, Benisch P, et al. Effects of high glucose on mesenchymal stem cell proliferation and differentiation. *Biochem Biophys Res Commun*. 2007;363(1):209-215. <https://doi.org/10.1016/j.bbrc.2007.08.161>.

48. Dhanasekaran M, Indumathi S, Rajkumar JS, Sudarsanam D. Effect of high glucose on extensive culturing of mesenchymal stem cells derived from subcutaneous fat, omentum fat and bone marrow. *Cell Biochem Funct.* 2013;31(1):20-29. <https://doi.org/10.1002/cbf.2851>.
49. Stolzing A, Coleman N, Scutt A. Glucose-induced replicative senescence in mesenchymal stem cells. *Rejuvenation Res.* 2006;9(1):31-35. <https://doi.org/10.1089/rev.2006.9.31>.
50. Khan WS, Adesida AB, Hardingham TE. Hypoxic conditions increase hypoxia-inducible transcription factor 2alpha and enhance chondrogenesis in stem cells from the infrapatellar fat pad of osteoarthritis patients. *Arthritis Res Ther.* 2007;9(3):R55. <https://doi.org/10.1186/ar2211>.
51. Koay EJ, Athanasiou KA. Hypoxic chondrogenic differentiation of human embryonic stem cells enhances cartilage protein synthesis and biomechanical functionality. *Osteoarthr Cartil.* 2008;16(12):1450-1456. <https://doi.org/10.1016/j.joca.2008.04.007>.
52. Stacpoole SRL, Spitzer S, Bilican B, et al. High yields of oligodendrocyte lineage cells from human embryonic stem cells at physiological oxygen tensions for evaluation of translational biology. *Stem Cell Rep.* 2013;1(5):437-450. <https://doi.org/10.1016/j.stemcr.2013.09.006>.
53. Mondragon-Teran P, Baboo JZ, Mason C, Lye GJ, Veraitch FS. The full spectrum of physiological oxygen tensions and step-changes in oxygen tension affects the neural differentiation of mouse embryonic stem cells. *Biotechnol Prog.* 2011;27(6):1700-1708. <https://doi.org/10.1002/btpr.675>.
54. Mondragon-Teran P, Lye GJ, Veraitch FS. Lowering oxygen tension enhances the differentiation of mouse embryonic stem cells into neuronal cells. *Biotechnol Prog.* 2009;25(5):1480-1488. <https://doi.org/10.1002/btpr.248>.
55. Park HH, Han MH, Choi H, et al. Mitochondria damaged by oxygen glucose deprivation can be restored through activation of the PI3K/Akt pathway and inhibition of calcium influx by amlodipine camsylate. *Sci Rep.* 2019;9:15717. <https://doi.org/10.1038/s41598-019-52083-y>.

How to cite this article: Esteban PP, Patel H, Veraitch F, Khalife R. Optimization of the nutritional environment for differentiation of human-induced pluripotent stem cells using design of experiments—A proof of concept. *Biotechnol Progress.* 2021;e3143. <https://doi.org/10.1002/btpr.3143>